Determination of the Geometric and Electronic Structure of Activated Bleomycin Using X-ray Absorption Spectroscopy

Tami E. Westre,† Kelly E. Loeb,† Jeffrey M. Zaleski,† Britt Hedman,*,‡ Keith O. Hodgson,*,†,‡ and Edward I. Solomon*,†

Contribution from the Department of Chemistry and Stanford Synchrotron Radiation Laboratory, Stanford University, Stanford, California 94305

Received August 24, 1994®

Abstract: Activated Bleomycin (BLM) is the first mononuclear non-heme iron oxygen intermediate stable enough for detailed spectroscopic study. DNA degradation by activated BLM involves C−H bond cleavage at the C4′ position of deoxyribose moieties and results in the production of base propenals. It has been postulated that activated BLM is an oxo−ferryl intermediate on the basis of its reactivity and analogy with cytochrome P-450 chemistry. Alternatively, spectroscopic and model studies have indicated activated BLM to have an iron(III)−peroxide site. In this study, X-ray absorption spectroscopy (XAS) has been used to *directly* probe the oxidation and spin states of the iron in activated BLM and to determine if a short iron−oxo bond is present, which would be characteristic of the oxo−ferryl species of heme iron. Both the pre-edge and edge regions of the Fe K-edge spectra indicate that activated BLM is a low spin ferric complex. The pre-edge intensity of activated BLM is also similar to that of low spin ferric BLM and does not show the intensity enhancement which would be present if there were a short Fe−O bond. Furthermore, bond distances obtained from EXAFS are similar to those in low spin Fe^{III}BLM and show no evidence for a short iron−oxo bond. These data indicate that activated BLM is a peroxy−low spin ferric complex and suggest that such an intermediate may play an important role in activating O_2 for further chemistry in the catalytic cycles of mononuclear non-heme iron enzymes.

Introduction

Bleomycin (BLM), a glycopeptide antibiotic produced by strains of *Streptomyces verticillus*, is currently used in treatment against a variety of carcinomas and lymphomas.[1] Its therapeutic activity involves selective DNA cleavage at certain GT and GC sites in the presence of metal ions (in particular Fe^{2+}) and dioxygen.[2,3] The coordination environment of the iron is believed to be square pyramidal with the iron ligated to five nitrogens from histidine, pyrimidine, a deprotonated peptide function, and primary and secondary amine groups.[4] Kinetic and spectral studies have demonstrated that the activation mechanism involves high spin Fe^{II}BLM reacting with dioxygen and an electron to form activated BLM which is formally at the peroxo−ferric level.[5] Activated BLM (and the analogous PMA model complex)[6] is the first mononuclear non-heme iron oxygen intermediate stable enough for detailed spectroscopic study. DNA degradation by activated BLM involves C−H bond cleavage at the C4′ position of deoxyribose moieties and results in the production of base propenals.[3,7] This mechanism is similar to the monooxygenation mechanism of cytochrome P-450 and has led researchers to postulate an oxo−ferryl BLM intermediate,[3] as has been generally considered to be present in P-450 chemistry. Alternatively, spectroscopic model studies[6,8] and mass spectrometric studies[9] have indicated activated BLM to have an iron(III)−peroxide site. In this study, X-ray absorption spectroscopy (XAS) has been used to directly probe the oxidation and spin state of the iron in activated BLM and to determine if a short iron−oxo bond is present which would be characteristic of the oxo−ferryl species of heme iron. Both the pre-edge and edge regions of the Fe K-edge spectra indicate that activated BLM is a low spin ferric complex. Bond distances obtained from extended X-ray absorption fine structure (EXAFS) are similar to those in low spin Fe^{III}BLM and show no evidence for a short iron−oxo bond. These data indicate that the iron(III)−peroxide formalism is an appropriate description of the iron center in activated BLM and suggest that such an intermediate may play an important role in activating O_2 for further chemistry in the catalytic cycles of mononuclear non-heme iron enzymes.

Experimental Section

Blenoxane (a mixture of 60% BLM A_2, 30% BLM B_2, and 10% other BLMs) was obtained as a gift from Bristol-Meyers Squibb and used without further purification. For all XAS samples a 5 mM apo-BLM solution consisting of equal volumes of 300 mM, pH 7.0, HEPES buffer (Sigma) and ethylene glycol (Mallinckrodt) was prepared. Subsequent anaerobic and aerobic additions of 5 μL of a $Fe(NH_4)_2(SO_4)_2{\cdot}6H_2O$ (FeAS; MCB Manufacturing Chemists, Inc.) stock solution yielded ~4 mM Fe^{II}BLM and Fe^{III}BLM, respectively. Sample integrity (<5% ferric impurity) was confirmed by optical absorption with an HP 8452A diode array spectrophotometer and by electron paramagnetic resonance (EPR) using a Bruker ER 220D-SRC spectrometer interfaced to an IBM XT computer and a Bruker ER 042MRH microwave bridge (X-band). The Fe^{II}BLM sample was syringed into the XAS sample cell (Lucite cell 23 × 1 × 3 mm with 37 μm Kapton windows) under a N_2 atmosphere and frozen in liquid N_2 before exposure to air.

† Department of Chemistry.
‡ Stanford Synchrotron Radiation Laboratory.
® Abstract published in *Advance ACS Abstracts*, January 1, 1995.

(1) Carter, S. K. *Bleomycin Chemotherapy*; Academic Press: New York, 1985; pp 3−35.
(2) Hecht, S. *Acc. Chem. Res.* **1986**, *19*, 383.
(3) Stubbe, J.; Kozarich, J. W. *Chem. Rev.* **1987**, *87*, 1107.
(4) Sugiura, Y. *Biochem. Biophys. Res. Commun.* **1979**, *87*, 643.
(5) Burger, R. M.; Peisach, J.; Horwitz, S. B. *J. Biol. Chem.* **1981**, *256*, 11636.
(6) Guajardo, R. J.; Hudson, S. E.; Brown, S. J.; Mascharak, P. K. *J. Am. Chem. Soc.* **1993**, *115*, 7971.
(7) McGall, G. H.; Rabow, L. E.; Ashley, G. W.; Wu, S. H.; Kozarich, J. W.; Stubbe, J. *J. Am. Chem. Soc.* **1992**, *114*, 4958.
(8) Burger, R. M.; Kent, T. A.; Horwitz, S. B.; Münck, E.; Peisach, J. *J. Biol. Chem.* **1983**, *258*, 1559.
(9) Sam, J. W.; Tang, X.-J.; Peisach, J. *J. Am. Chem. Soc.* **1994**, *116*, 5250.

0002-7863/95/1517-1309$09.00/0

Activated BLM was formed from the reaction of low spin Fe^{III}BLM with H_2O_2 (Mallinckrodt)[5] because the reaction of Fe^{II}BLM with O_2 yields a 50:50 mixture of activated BLM and low spin Fe^{III}BLM. The intermediate was prepared at 4 °C by rapid addition of 3.8 μL of H_2O_2 (100-fold excess) to 80 μL of Fe^{III}BLM followed by simultaneous freezing in the XAS sample cell and a 3 mm EPR tube after a 25 s incubation. This method resulted in samples with superimposable EPR spectra. The concentrations of the individual components of the activated BLM sample were determined by spin-quantitation of the sample in the EPR tube using a 1 mM $CuSO_4 \cdot 5H_2O$ (Mallinckrodt) solution in 2 mM HCl and 2 M $NaClO_4$ (Fisher), and a 3 mM Fe^{III}-EDTA solution in 50/50 glycerol (Baker)/water (prepared by stirring $Fe^{III}Cl_3 \cdot 6H_2O$ (Baker) with excess $Na_2EDTA \cdot 2H_2O$ (Aldrich) for 12 h) as standards in the $g = 2.0$ and $g = 4.3$ regions, respectively. The proportionality of the high field feature in the Fe^{III}BLM EPR spectrum ($g = 1.89$) to the total low spin ferric signal was used to account for this contribution to the overlapping features in the EPR spectrum of the intermediate and to quantitate the remaining low spin signal attributed to activated BLM. Quantitation of the EPR silent degradation product was achieved by subtracting the percentages of the EPR detectable components from the total Fe^{III}BLM concentration determined by quantitation of the sample prior to activation and accounting for the 3.8 μL H_2O_2 dilution. This revealed a sample composed of 81(4)% activated BLM, 7(1)% low spin Fe^{III}BLM, 4(1)% high spin ferric, and 8(1)% Fe degradation product undetectable by EPR at 77 K. A separate sample with the degradation product of the Fe^{III}BLM−H_2O_2 reaction was generated by allowing activated BLM to decay for 12 h, producing 8% high spin ferric with the remaining 92% Fe EPR silent at 77 K.

X-ray absorption spectra were recorded at the Stanford Synchrotron Radiation Laboratory on unfocused wiggler beamline 7-3 during dedicated conditions (3 GeV, 50−100 mA). The radiation was monochromatized using a Si(220) double-crystal monochromator. An Oxford Instruments continuous-flow liquid helium CF1208 cryostat was used to maintain a constant temperature of 10 K. Energies were calibrated using an internal Fe foil standard, assigning the first inflection point to 7111.2 eV.[10] The spectrometer energy resolution was approximately 1.5 eV with reproducibility in edge position determination of <0.2 eV.

Data were collected on Fe^{II}BLM, Fe^{III}BLM, 81(4)% activated BLM, and the degradation product of the Fe^{III}BLM−H_2O_2 reaction. Data were measured to $k = 15$ Å^{-1} with 1 mm high premonochromator beam-defining slits, detuning the monochromator 50% at 7998 eV to minimize harmonic contamination. The fluorescence signal was monitored by using a 13-element Ge solid-state array detector[11] windowed on the Fe Kα signal. During the experiment, count rates of approximately 30 000 s^{-1} total per element were not exceeded. Approximately 30 scans were averaged for each sample. A smooth pre-edge background was removed from the averaged spectra by fitting a second order polynomial to the pre-edge region and subtracting this polynomial from the entire spectrum. A three-segment spline approximately even in k-space was fit to the EXAFS region and the data normalized to an edge jump of 1 at 7130 eV. The spline was chosen so that it minimized residual low-frequency background but did not reduce the EXAFS amplitude as checked by monitoring the Fourier transform of the EXAFS during the background subtraction process.

Fe K-edge spectra were also collected on several iron model complexes. $[Fe(Prpep)_2] \cdot 2CH_3OH$ and $[Fe(Prpep)_2]ClO_4 \cdot 2CH_3OH \cdot CH_3CN$ were obtained as gifts from P. Mascharak.[12] $[Fe(imidazole)_6]Cl_2$[13] and $Na[Fe(H_2O)EDTA]$[14] were prepared as previously described. $[Fe(Prpep)_2] \cdot 2CH_3OH$, $[Fe(Prpep)_2]ClO_4 \cdot 2CH_3OH \cdot CH_3CN$, and $[Fe(imidazole)_6]Cl_2$ are air-sensitive, and thus the following procedure was carried out in a nitrogen-filled glovebox. The crystalline samples were each mixed with boron nitride (BN) and ground into a fine powder. The BN/sample mixture was pressed into a 1 mm thick Al spacer that was sealed with 63.5 μm Mylar tape windows and frozen in liquid nitrogen. Data were measured in transmission mode with N_2-filled ionization chambers to $k = 9.5$ Å^{-1}, detuning the monochromator 50% at 7474 eV to minimize harmonic contamination. Two to three scans were averaged for each sample. A smooth pre-edge background was removed from the averaged spectra by fitting a first-order polynomial to the pre-edge region and subtracting this polynomial from the entire spectrum. A two-segment spline of order 2 was fit to the EXAFS region, and the data were normalized to an edge jump of 1 at 7130 eV.

EXAFS data reduction was performed on the normalized BLM spectra according to established methods.[15−17] The normalized data were converted to k-space. The photoelectron wave vector, k, is defined by $[2m_e(E - E_0)/\hbar^2]^{1/2}$, where m_e is the electron mass, E is the photon energy, $\hbar$ is Planck's constant divided by 2π, and E_0 is the threshold energy of the absorption edge, which was defined to be 7130 eV for the Fe K absorption edge. The empirical EXAFS data analyses were performed with nonlinear least-squares curve-fitting[10,15−17] techniques using empirical phase and amplitude parameters. The following models were used to obtain the empirical Fe−X backscattering parameters of interest: Fe−O from $[Fe(acetylacetonate)_3]$[18,19] and Fe−N from $[Fe(1,10\text{-phenanthroline})_3](ClO_4)_3$.[20,21] Fourier transforms (from k- to R-space) were performed for the data range 3.5−12.5 Å^{-1} with a Gaussian window of 0.1 Å^{-1}. The window widths used in the back-transforms (from R- to k-space) for the BLM samples are given in the results and discussion section. The window widths were kept as similar as possible to those used to extract amplitude and phase parameters from the model compounds to minimize artifacts introduced by the Fourier filtering technique. All curve-fitting was based on k^3-weighted data and applied to the individual filtered shell of interest. Only the structure-dependent parameters, the distance and coordination number, were varied unless stated otherwise. A "goodness of fit" parameter, F, was calculated as $F = \{[k^6(\text{data} - \text{fit})^2]/(\text{no. of points})\}^{1/2}$ for each fit.

Contributions to the XAS spectrum due to low spin Fe^{III}BLM and degradation product were subtracted from the normalized data of the 81% activated BLM spectrum to obtain a 96% activated BLM spectrum. As stated above, all the averaged spectra were normalized to an edge jump of 1. Fe^{III}BLM and degradation product data were used to subtract 7% and 8%, respectively, from the normalized 81% activated BLM spectrum, giving a 96% pure activated BLM spectrum which was then renormalized to an edge jump of 1. The remaining 4% corresponds to a high spin ferric impurity for which no reference is available. The 96% activated BLM edge spectrum was identical in shape to that of the 81% pure sample; however, the edge shifted 0.7 eV to higher energy. The 96% activated BLM spectrum was used in the edge analysis, whereas the original 81% activated BLM spectrum was used in the EXAFS analysis.

Results and Discussion

Fe K-Edge XAS. The Fe K-edge spectra of Fe^{II}BLM, Fe^{III}-BLM, and activated BLM are shown in Figure 1A, whereas Figure 1B shows an expanded view of the 1s → 3d pre-edge region. The lowest energy peaks arise from the weak 1s → 3d transition at ~7113 eV followed by the 1s → 4p transition at ~7122 eV. The spectrum of Fe^{II}BLM (solid line) has two low-intensity pre-edge peaks at 7111.4 and 7113.6 eV (Figure 1B). The data for both Fe^{III}BLM (dashed line) and activated BLM (dotted line) have similar pre-edge features, each with a maximum at 7112.5 eV with similar intensity, a barely resolvable low energy shoulder for Fe^{III}BLM at ~7111 eV, and a

(10) Scott, R. A.; Hahn, J. E.; Doniach, S.; Freeman, H. C.; Hodgson, K. O. *J. Am. Chem. Soc.* **1982**, *104*, 5364.
(11) Cramer, S. P.; Tench, O.; Yochum, M.; George, G. N. *Nucl. Instrum. Methods Phys. Res.* **1988**, *A266*, 586.
(12) PrpepH = *N*-(2-(4-imidazole)ethyl)pyrimidine-4-carboxamide.
(13) Burbridge, C. D.; Goodgame, D. M. L. *Inorg. Chim. Acta* **1970**, *4*, 231.
(14) Lind, M. D.; Hamor, M. J.; Hamor, T. A.; Hoard, J. *Inorg. Chem.* **1963**, *3*, 34.
(15) Cramer, S. P.; Hodgson, K. O.; Stiefel, E. I.; Newton, W. E. *J. Am. Chem. Soc.* **1978**, *100*, 2748.
(16) Cramer, S. P.; Hodgson, K. O. *Prog. Inorg. Chem.* **1979**, *15*, 1.
(17) Scott, R. A. *Methods Enzymol.* **1985**, *117*, 414.
(18) Roof, R. B. J. *Acta Crystallogr.* **1967**, *9*, 781.
(19) Iball, J.; Morgan, C. H. *Acta Crystallogr.* **1967**, *23*, 239.
(20) Johansson, L. *Chem. Scr.* **1976**, *9*, 30.
(21) The crystal structure of the perchlorate salt has not been determined, but the $[Fe(phenanthroline)_3]^{2+}$ complex structure can be assumed to be identical with that of the corresponding iodide salt (Johansson, L.; Molund, M.; Oskarsson, Å. *Inorg. Chim. Acta* **1978**, *31*, 117).

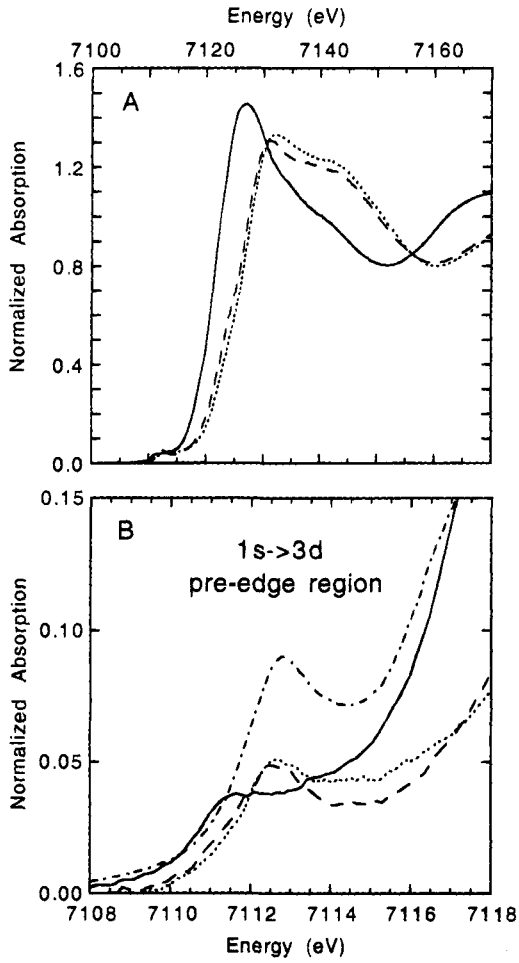

Figure 1. (A) Fe K XAS edge spectra of Fe^{II}BLM (—), Fe^{III}BLM (- - -), and activated BLM (•••). (B) Expansion of the 1s → 3d pre-edge region of part A with pre-edge data of $Fe(Me_3TACN)(NO)(N_3)_2$ (— • —), which has an Fe—N(O) bond of 1.74 Å.

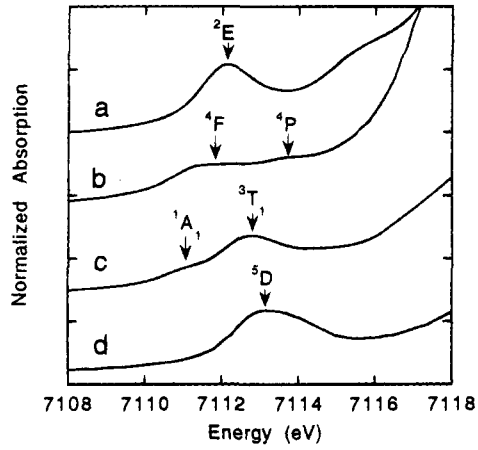

Figure 2. The 1s → 3d pre-edge region of representative iron model complexes: (a) low spin ferrous complex, $[Fe(Prpep)_2]\cdot 2CH_3OH$; (b) high spin ferrous complex, $[Fe(imidazole)_6]Cl_2$; (c) low spin ferric complex, $[Fe(Prpep)_2]ClO_4\cdot 2CH_3OH\cdot CH_3CN$; (d) high spin ferric complex, $Na[Fe(H_2O)EDTA]$. The individual spectra are offset vertically by increments of 0.05 on the *y*-scale.

sloping tail in this lower energy region in activated BLM. The rising edge inflection points occur at 7121.3 eV for Fe^{II}BLM, 7127.0 eV for Fe^{III}BLM, and 7127.3 eV for activated BLM. Figure 2 contains the 1s → 3d pre-edge region for representative iron model complexes: (a) a low spin ferrous complex, $[Fe(Prpep)_2]\cdot 2CH_3OH$;[22] (b) a high spin ferrous complex, $[Fe(imidazole)_6]Cl_2$;[13] (c) a low spin ferric complex, $[Fe(Prpep)_2]ClO_4\cdot 2CH_3OH\cdot CH_3CN$;[22] and (d) a high spin ferric complex, $Na[Fe(H_2O)EDTA]$.[14] The $[Fe(Prpep)_2]\cdot 2CH_3OH$ spectrum has a single peak in the pre-edge region located at 7112.1 eV, while the $[Fe(imidazole)_6]Cl_2$ spectrum has features at 7111.3 and 7113.6 eV. The data for $[Fe(Prpep)_2]ClO_4\cdot 2CH_3OH\cdot CH_3CN$ also show two pre-edge features, a low energy shoulder at 7111.0 eV and a more intense peak at 7112.7 eV. The pre-edge feature of $Na[Fe(H_2O)EDTA]$ has a maximum at 7112.9 eV with a higher energy shoulder.

The energy of the edge position (dominated by the 1s → 4p transition) is dependent upon the effective nuclear charge of the absorbing metal atom. This charge is governed by a combination of effects, including the formal metal oxidation state, the number and type of ligating atoms, and the coordination geometry.[23-28] In this case, the types of ligating atoms and the coordination sphere are similar; thus changes in the edge energy can be correlated to the iron oxidation state. From Figure 1A, the edge spectrum of activated BLM is very close in energy and similar in shape to that of Fe^{III}BLM, in contrast to the Fe^{II}-BLM spectrum which is ~6 eV lower in energy and has a more intense 1s → 4p feature, indicating that activated BLM contains a ferric metal center. It should be noted that the edge inflection point of horseradish peroxidase compound I, which has a purported Fe(IV)=O metal site, was observed to be at ~2 eV higher in energy than that of the resting ferric horseradish peroxidase.[29]

The 1s → 3d pre-edge feature can be used to probe the spin and oxidation states of the iron site in activated BLM since the final state ($1s^13d^{n+1}$) has a different multiplet splitting for high spin ferrous (^4F,^4P), high spin ferric (^5D), low spin ferrous (^2E), and low spin ferric ($^1A_1$, $^3T_1$) cases. The number, intensity ratio, and energies of the pre-edge multiplet features are indicative of the specific oxidation and spin states of the iron. As can be seen in Figure 2, the low spin ferrous complex has a single pre-edge feature which has a maximum at ~7112 eV (Figure 2a), while high spin ferrous complexes have two features split by 2 eV (Figure 2b). This correlates with the fact that there is a single allowed final state for low spin ferrous complexes (^2E) while there are two final states of maximum spin multiplicity for the high spin ferrous complexes (^4F,^4P). In the free atom, the ^4F and ^4P states are split by ~2 eV.[24] A typical pre-edge for a low spin ferric complex has a maximum at ~7112.5 eV with a lower energy shoulder at ~7111 eV, corresponding to transitions to $^3T_1$ and $^1A_1$, respectively (Figure 2c). The magnitude of this splitting is of the same order as the energy resolution of this experiment. Thus, a distinct low energy shoulder is not always observed, especially for complexes that have somewhat lower ligand field strengths and hence a smaller splitting between the $^3T_1$ and $^1A_1$ states. There is one final state of maximum spin multiplicity allowed for high spin ferric complexes, the ^5D state. However, this state splits into the $^5T_2$ and ^5E states as the ligand field strength increases. Thus, high spin ferric complexes usually have a pre-edge feature at ~7113

(22) Brown, S. J.; Olmstead, M. M.; Mascharak, P. K. *Inorg. Chem.* **1990**, *29*, 3229.
(23) Srivastave, U. C.; Nigam, H. L. *Coord. Chem. Rev.* **1973**, *9*, 275.
(24) Shulman, R. G.; Yafet, Y.; Eisenberger, P.; Blumberg, W. E. *Proc. Natl. Acad. Sci. U.S.A.* **1976**, *73*, 1384.
(25) Cramer, S. P.; Eccles, T. K.; Kutzler, F. W.; Hodgson, K. O. *J. Am. Chem. Soc.* **1976**, *98*, 1287.
(26) Wong, J.; Lytle, F. W.; Messmer, R. P.; Maylotte, D. H. *Phys. Rev. B* **1984**, *30*, 5596.
(27) Roe, A. L.; Schneider, D. J.; Mayer, R. L.; Pyrz, J. W.; Widom, J.; Que, L., Jr. *J. Am. Chem. Soc.* **1984**, *106*, 1676.
(28) Kau, L. S.; Spira-Solomon, D. J.; Penner-Hahn, J. E.; Hodgson, K. O.; Solomon, E. I. *J. Am. Chem. Soc.* **1987**, *109*, 6433.
(29) Penner-Hahn, J. E.; McMurry, T. J.; Renner, M.; Latos-Grazynsky, L.; Eble, K. S.; Davis, I. M.; Balch, A. L.; Groves, J. T.; Dawson, J. H.; Hodgson, K. O. *J. Biol. Chem.* **1983**, *258*, 12761.

eV with a second feature barely resolvable in complexes with a large $10Dq$ splitting (Figure 2d). The splitting of the pre-edge in Fe^{II}BLM (Figure 1B solid line) is attributed to the ^4F and ^4P ferrous ion splitting of ~2 eV.[24] Fe^{III}BLM and activated BLM both exhibit a pre-edge with maximum at 7112.5 eV with a lower energy shoulder being barely resolved in the Fe^{III}BLM data. The energy position of the pre-edge features and the shape of both the Fe^{III}BLM and the activated BLM indicate that both complexes have a low spin ferric active site.

The pre-edge features can also provide information on the geometric structure of the active site. The 1s → 3d pre-edge feature is formally electric dipole forbidden but gains intensity through an allowed quadrupole transition and through 4p mixing into the 3d states as a result of the noncentrosymmetric environment of the metal site. When the symmetry of the iron site is lowered, the pre-edge intensity increases due to an increase in the 3d-4p mixing.[27] Iron−oxo[30] and iron−nitrosyl[31] complexes typically have pre-edge features that are a factor of 2 more intense than their centrosymmetric counterparts due to their short ~1.8 Å Fe−O/N bond. See, for example, the factor of 2 increase for $Fe(Me_3TACN)(NO)(N_3)_2$[32] (where TACN = *N,N′,N″*-trimethyl-1,4,7-triazacyclononane) which has been included in Figure 1B (dot dashed line) as a reference. This iron−nitrosyl complex has an Fe−N(O) bond length of 1.74 Å. The pre-edge intensity of a five-coordinate oxo−ferryl porphyrin complex with an Fe−O bond of 1.65 Å is even greater than that of $Fe(Me_3TACN)(NO)(N_3)_2$ due to the shorter Fe−O bond length.[33] In contrast, the spectrum of activated BLM (Figure 1B dotted line) has a pre-edge intensity which is typical of a six-coordinate low spin ferric complex with no severe distortion around the iron site, eliminating the possibility of a short Fe−O bond.

EXAFS. The EXAFS spectra of Fe^{II}BLM, Fe^{III}BLM, and activated BLM are shown in Figure 3A and the Fourier transforms (FTs), taken over the k range of 3.5−12.5 $Å^{-1}$, are shown in Figure 3B. Curve-fitting was performed on filtered first shell contributions over the k range 4−12 $Å^{-1}$ varying bond distances and coordination numbers. The results of the curve-fitting are presented in Table 1 with the best fits shown in Figure 4. The first shell of each sample could not be adequately fit with a single low-Z wave (fits 1, 3, and 5 in Table 1). The Fe^{II}BLM data were well fit by two shells of N atoms (fit 2 in Table 1 and Figure 4) with an average Fe−N distance of 2.16 Å. The Fe^{III}BLM and activated BLM data were also fit with two shells of low Z atoms (fits 4 and 6 in Table 1 and Figure 4) but with an average first shell distance 0.2 Å shorter than in Fe^{II}BLM (see Fourier transforms in Figure 3B). The two N shells from the fit to the Fe^{III}BLM and activated BLM data have very similar distances with slight changes in the coordination numbers consistent with both being low spin ferric complexes. In contrast, an oxo−ferryl species would have a bond length of ~1.65 Å.[29] The presence of a short Fe−O was further examined by fixing Fe−O distances of 1.65 and 1.75 Å with a coordination number of 1, while varying the coordination numbers and distances of the two longer shells of N. These fits to the data do not support a shorter Fe−O distance in that there was a much worse fit to the data when a 1.65 or 1.75 Å contribution was added (fit 7, Figure 4), and the coordination numbers of the other N shells became unreasonable (total CN of ~11). When the third shell distance was allowed to vary, it refined to a value of 1.83 Å with the fit having a similar F value as fit 6 (Table 1). These studies indicate that an oxo−ferryl species is clearly not present from the analysis of the EXAFS data.

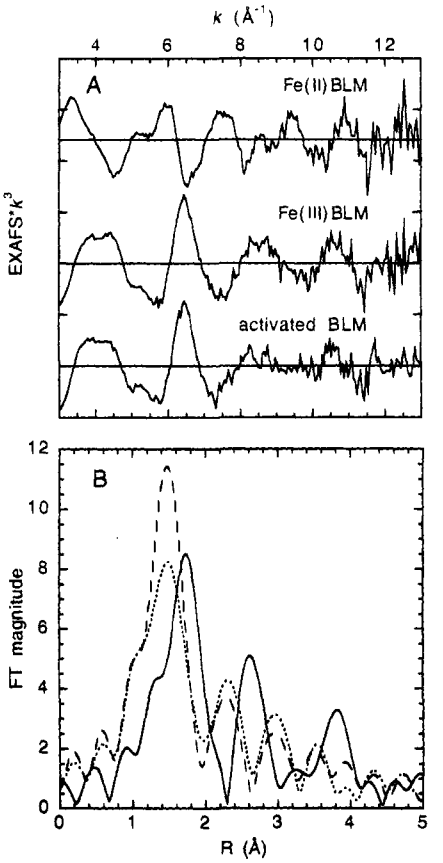

Figure 3. (A) EXAFS data ($*k^3$) for Fe^{II}BLM, Fe^{III}BLM, and activated BLM (the ordinate scale is 5 between major tick marks on an absolute scale with solid horizontal lines indicating the zero-point of each plot). (B) Fourier transforms (non-phase-shift-corrected) over the k-range 3.5−12.5 $Å^{-1}$ of the EXAFS data for Fe^{II}BLM (—), Fe^{III}BLM (- - -), and activated BLM (•••).

Table 1. Summary of EXAFS Curve-Fitting Results

sample	Fit no.	FT window width (Å)	element	CN[a,b]	bond length (Å)[b]	F
Fe^{II}BLM	1	[1.0−2.25]	N	3.0	2.16	0.41
	2	[1.0−2.25]	N	1.4	2.08	0.29
			N	3.0	2.19	
Fe^{III}BLM	3	[0.75−2.0]	N	3.3	1.94	0.73
	4	[0.75−2.0]	N	3.4	1.90	0.31
			N	2.5	2.03	
activated BLM	5	[0.7−2.0]	N	2.5	1.96	0.84
	6	[0.7−2.0]	N	2.5	1.89	0.36
			N	3.0	2.03	
	7	[0.7−2.0]	O	1*	1.65*	0.75
			N	7.0	1.91	
			N	2.9	2.07	

[a] CN = coordination number. [b] Errors in distances (±0.02 Å) and coordination numbers (±25%) are estimated from the variance between EXAFS fitting results and values from models of crystallographically known structure.[15] * values fixed.

Conclusion

Both the energy position and shape of the rising edge of the activated BLM XAS spectrum are very similar to those for Fe^{III}-BLM, indicating that the iron in activated BLM is ferric. Both Fe^{III}BLM and activated BLM exhibit a weak pre-edge feature at 7112.5 eV with a lower energy shoulder indicative of a low

(30) Dewitt, J. Ph.D. Dissertation, Stanford University, Stanford, CA, 1993.
(31) Zhang, Y.; Pavlosky, M. A.; Brown, C. B.; Westre, T. E.; Hedman, B.; Hodgson, K. O.; Solomon, E. I. *J. Am. Chem. Soc.* **1992**, *114*, 9189.
(32) Pohl, K.; Wieghardt, K.; Nuber, B.; Weiss, J. *J. Chem. Soc., Dalton Trans.* **1987**, 187.
(33) Liu, H. I.; Gold, A.; Dawson, J. H.; Hedman, B.; Hodgson, K. O. Unpublished data.

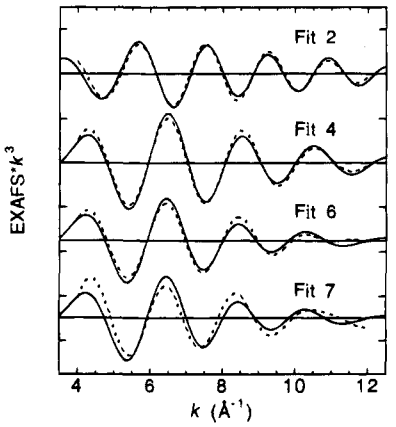

Figure 4. Empirical first shell fits to the Fourier-filtered EXAFS data with the solid lines representing the experimental data and the dashed line representing the fit to the data. Fits 2, 4, and 6 are the best empirical fits to the Fe^{II}BLM, Fe^{III}BLM, and activated BLM data, respectively. Fit 7 is a fit to the activated BLM data where a short 1.65 Å Fe−O bond distance was included. (The ordinate scale is 4 between major tick marks on an absolute scale with solid horizontal lines indicating the zero point of each plot.)

spin ferric active site with no severe distortion (*i.e.*, no short iron−oxo bond). The first shell distances obtained from the EXAFS data of activated BLM are within 0.01 Å of the Fe^{III}-BLM distances with slight changes in the coordination numbers. Thus, the XAS data of activated BLM are *not* consistent with a Fe(IV)=O species but rather with a low spin ferric peroxide description of the active site. These results confirm the description of activated BLM being a peroxy−Fe^{III}BLM species presented in a recent mass spectrometry study.[9] Our results provide a *direct* determination of both the iron oxidation and spin states and the fact that there is no short iron−oxo bond. Activated BLM is the first mononuclear non-heme iron oxygen intermediate to be characterized, and its description suggests that such a peroxy−ferric complex may play an important role in O_2 activation by this class of enzymes. Experiments are currently underway to define the peroxide binding mode and to generate a detailed electronic structure description of activated BLM in order to understand the nature of the oxygen activation.

Acknowledgment. This research is supported by grants from the NIH (GM40392, E.I.S.) and NSF (CHE-9121576, K.O.H.). SSRL is supported by the U.S. Department of Energy, Office of Basic Energy Science, Divisions of Chemical and Materials Sciences, and in part by the National Institutes of Health, Biomedical Research Technology Program (RR-01209) and the U.S. Department of Energy, Office of Health and Environmental Research. J.M.Z. thanks the Jane Coffin Childs Fund for Medical Research for a postdoctoral fellowship.

JA942839I